A method for the deconvolution of incompletely resolved CARS spectra in chemical dynamics experiments

Andrew A. Anda, David L. Phillips, and James J. Valentini

Citation: The Journal of Chemical Physics **85**, 1719 (1986); doi: 10.1063/1.451172
View online: http://dx.doi.org/10.1063/1.451172
View Table of Contents: http://scitation.aip.org/content/aip/journal/jcp/85/4?ver=pdfcov
Published by the AIP Publishing

A method for the deconvolution of incompletely resolved CARS spectra in chemical dynamics experiments

Andrew A. Anda[a)]
Chemistry Division, Los Alamos National Laboratory, Los Alamos, New Mexico 87545

David L. Phillips and James J. Valentini
Department of Chemistry, University of California, Irvine, California 92717

(Received 14 April 1986; accepted 9 May 1986)

We describe a method for deconvoluting incompletely resolved CARS spectra to obtain quantum state population distributions. No particular form for the rotational and vibrational state distribution is assumed, the population of each quantum state is treated as an independent quantity. This method of analysis differs from previously developed approaches for the deconvolution of CARS spectra, all of which assume that the population distribution is Boltzmann, and thus are limited to the analysis of CARS spectra taken under conditions of thermal equilibrium. The method of analysis reported here has been developed to deconvolute CARS spectra of photofragments and chemical reaction products obtained in chemical dynamics experiments under nonequilibrium conditions. The deconvolution procedure has been incorporated into a computer code. The application of that code to the deconvolution of CARS spectra obtained for samples at thermal equilibrium and not at thermal equilibrium is reported. The method is accurate and computationally efficient.

I. INTRODUCTION

In recent years coherent anti-Stokes Raman scattering (CARS) spectroscopy has found numerous applications as a probe of rotational and vibrational state populations of molecules in flames, internal combustion and jet engines, electric discharges and plasmas, and chemically reacting mixtures.[1] In our laboratory CARS spectroscopy is being used in chemical dynamics experiments to measure electronic, vibrational, and rotational state distributions of photofragments and reaction products under single-collision conditions.[2–6]

The type of spectrum most frequently obtained in CARS spectroscopy is the vibrational Q-branch spectrum, corresponding to transitions $v, J \rightarrow v+1, J$. Transitions with different values of J occur at different transition frequencies only because the rotational constants B_v and B_{v+1} differ. For strongly bound molecules (e.g., N_2, O_2, CO, etc.) in low vibrational states the difference $B_v - B_{v+1}$ is quite small, of the order of 0.01 cm^{-1}, so the Q-branch transitions from different rotational states are quite closely spaced. Often, the observed CARS spectrum is not completely rotationally resolved, because the linewidths of the lasers used to obtain the spectrum are comparable to or greater than the spacing between adjacent rotational transitions.

For such incompletely resolved spectra some spectral deconvolution must be performed in order to extract the rotational and vibrational population distributions. This deconvolution can be quite complicated. Because CARS is a nonlinear process, the signal amplitudes from neighboring transitions can interfere constructively or destructively when the laser linewidth is great enough to access them simultaneously. As a result, the CARS signal intensity is not simply a sum over the intensities of all the transitions lying under the laser line profile. However, the deconvolution is a mathematically soluble and computationally tractable problem.

The deconvolution problem is simplified if the rotational and vibrational populations are known to follow a Boltzmann distribution. In this case there is only one unknown—the temperature—in the deconvolution, while there are many data—the CARS spectral intensities at each of the transition frequencies. Given information about the transition linewidths, laser linewidths, Raman cross sections, etc., one can treat the temperature as a fitting parameter of the spectrum, adjusting it until agreement between a computed and the observed spectrum is achieved. Methods for performing such analysis of CARS spectra of molecules having Boltzmann distributions have been developed, because of the widespread use of CARS for thermometry in combustion media. One widely used approach is that developed by Hall.[7]

The photofragments and reaction products whose CARS spectra are obtained under single-collision conditions in chemical dynamics experiments cannot be assumed to have Boltzmann rotational and vibrational distributions. Nor can it be assumed that the quantum state populations follow any other particular functional form. When the CARS spectra of such species are incompletely resolved, the deconvolution thus must treat the populations in each rotational–vibrational state as independent unknown quantities. The deconvolution then is a problem of n unknowns determined by n equations, and requires a different method of solution from that used for CARS thermometry applications.

This paper presents a methodology for the deconvolution of CARS spectra of molecules with non-Boltzmann population distributions. It has been developed primarily for

[a)] Present address: 5635 N. Kostner Ave., Chicago, Illinois 60646.

 0021-9606/86/161719-07$02.10

the deconvolution of CARS spectra obtained in chemical dynamics experiments. However, it is generally applicable and should prove useful for the analysis of CARS spectra obtained in any sample that cannot be assumed to be at thermal equilibrium, for example, in discharges, laser media, chemical vapor deposition, chemical etching, etc. Section II below describes the nature of the problem and a brief review of the phenomenonology of CARS, while Sec. III presents the mathematical formalism and algorithm used in our method of solution. The description of the Fortran computer code which embodies this formalism also is given in Sec. III. Section IV presents examples of the application of this computer code for CARS spectral deconvolution, and finally, Sec. V summarizes our conclusions regarding the methodology.

II. NATURE OF THE PROBLEM

An electric field $\mathbf{E}$ induces in a molecule or atom an electric dipole moment which may be expressed as[8]

$$\boldsymbol{\mu} = \boldsymbol{\alpha}\mathbf{E} + \boldsymbol{\beta}\mathbf{E}^2 + \boldsymbol{\gamma}\mathbf{E}^3 + \cdots . \tag{1}$$

The induced dipole vector can point in a direction different from that of the electric field vector, so the coefficients α, β, γ, etc. are tensor quantities. The polarizability α is a rank 2 tensor, while the hyperpolarizabilities β, γ, ... are rank 3, 4, ... tensors, respectively. A substance exhibits a bulk polarization due to the dipole moment induced in its component atoms or molecules. This polarization $\mathbf{P}$ may be written as

$$\mathbf{P} = \chi^{(1)}\mathbf{E} + \chi^{(2)}\mathbf{E}^2 + \chi^{(3)}\mathbf{E}^3 + \cdots , \tag{2}$$

where $\chi^{(1)}$, $\chi^{(2)}$, $\chi^{(3)}$, ... are the first-order, second-order, third-order, ... dielectric susceptibility tensors. The induced dipole moment $\boldsymbol{\mu}$ and the polarization $\mathbf{P}$ are related by the equation

$$\mathbf{P} = N\zeta\boldsymbol{\mu} , \tag{3}$$

where N is the particle density and ζ is a factor relating the applied macroscopic field to the field acting on the individual particles.[9-11] For substances such as gases, which have an optical index of refraction near unity, the two fields are almost the same, so

$$\mathbf{P} = N\boldsymbol{\mu} , \tag{4}$$

and

$$\begin{aligned} \chi^{(1)} &= N\alpha , \\ \chi^{(2)} &= N\beta , \\ \chi^{(3)} &= N\gamma . \end{aligned} \tag{5}$$

The third-order dielectric susceptibility tensor $\chi^{(3)}$ gives rise to CARS[1] as well as other effects like third harmonic generation. In CARS, electric fields at frequencies ω_1, ω_2, and ω_3 generate a polarization and a resultant signal at frequency ω_0, given by

$$\omega_0 = \omega_1 - \omega_2 + \omega_3 , \tag{6}$$

due to a third-order term $\chi^{(3)}\mathbf{E}(\omega_1)\mathbf{E}(\omega_2)\mathbf{E}(\omega_3)$. Often, only two field frequencies are used, and $\omega_1 = \omega_3$, so

$$\omega_0 = 2\omega_1 - \omega_2 = \omega_1 + (\omega_1 - \omega_2) , \tag{7}$$

and $\mathbf{P}^{\mathrm{CARS}} = \chi^{(3)}\mathbf{E}^2(\omega_1)\mathbf{E}(\omega_2)$. For a Raman transition of frequency $\omega_{rg} = (E_g - E_r)/\hbar$ the CARS process will be Raman resonant when

$$\omega_1 - \omega_2 = \omega_{rg} , \tag{8}$$

and then

$$\omega_0 = \omega_1 + \omega_{rg} , \tag{9}$$

$$\omega_2 = \omega_1 - \omega_{rg} . \tag{10}$$

Hence, ω_0 is commonly referred to as the anti-Stokes frequency, while ω_2 is termed the Stokes frequency. The frequency ω_1 is called the pump frequency. The CARS signal is

$$I(\omega_0) \propto |\chi^{(3)}|^2 I^2(\omega_1) I(\omega_2) , \tag{11}$$

where $I(\omega_i)$ is the intensity of the field at frequency ω_i. A CARS spectrum can be obtained by scanning the frequency of the Stokes laser while keeping fixed the frequency of the pump laser.

$\chi^{(3)}$ may be written as a sum of Raman resonant and nonresonant parts, with the resonant part made up of real and imaginary components:

$$\chi^{(3)} = \chi' + i\chi'' + \chi^{\mathrm{NR}} , \tag{12}$$

where we have suppressed the tensor nature of $\chi^{(3)}$.

The real and imaginary components χ' and χ'' of the resonant susceptibility may be expressed as

$$\chi' = \frac{\Delta N_{rg} c^4}{\hbar\omega_2^4} \frac{d\sigma}{d\Omega} \frac{\omega_{rg}\left[\omega_{rg}^2 - (\omega_1 - \omega_2)^2\right]}{\left[\omega_{rg}^2 - (\omega_1 - \omega_2)^2\right]^2 + \Gamma_{rg}^2(\omega_1 - \omega_2)^2} \tag{13}$$

and

$$\chi'' = \frac{\Delta N_{rg} c^4}{\hbar\omega_2^4} \frac{d\sigma}{d\Omega} \frac{\omega_{rg}\,\Gamma_{rg}(\omega_1 - \omega_2)}{\left[\omega_{rg}^2 - (\omega_1 - \omega_2)^2\right]^2 + \Gamma_{rg}^2(\omega_1 - \omega_2)^2} , \tag{14}$$

where $d\sigma/d\Omega$ is the Raman differential scattering cross section, c is the speed of light, ω_1 is the pump frequency, ω_2 is the Stokes frequency, and ω_{rg} is the frequency of the Raman transition between the r and g energy levels. Γ_{rg} is the Raman linewidth for the transition and ΔN_{rg} is the population difference between the r and g energy levels,

$$\Delta N_{rg} = N_r - N_g . \tag{15}$$

We assume χ^{NR} is real and independent of ω_0, ω_1, and ω_2.

Note that while χ'' is an even function of $\omega_1 - \omega_2$ centered at ω_{rg}, χ' is an odd function of $\omega_1 - \omega_2$, and the phase of χ' depends on the sign of ΔN_{rg}. The lasers which provide ω_1 and ω_2 have finite frequency width, which usually is not small compared to the spacing of the Raman lines. In this case the CARS laser fields at ω_1 and ω_2 are simultaneously resonant with more than one Raman transition. A commonly encountered example of this occurs for the rotational transitions in a vibrational Q-branch Raman band. These adjacent transitions will interfere with one another, due to cross terms in $\chi^{(3)}$. For n Raman resonances, $\chi^{(3)}$ is given by

$$\chi^{(3)} = \sum_{j=1}^{n} (\chi_j' + i\chi_j'') + \chi^{\mathrm{NR}} . \tag{16}$$

For three resonances this expands to

$$\chi^{(3)} = \chi_1' + i\chi_1'' + \chi_2' + i\chi_2'' + \chi_3' + i\chi_3'' + \chi^{\mathrm{NR}} , \tag{17}$$

and we find

$$
\begin{aligned}
&|\chi^{(3)}|^2 \\
&= (\chi_1')^2 + (\chi_2')^2 + (\chi_3')^2 + (\chi_1'')^2 + (\chi_2'')^2 + (\chi_3'')^2 \\
&\quad + 2\chi_1'\chi_2' + 2\chi_1'\chi_3' + 2\chi_2'\chi_3' + 2\chi_1''\chi_2'' + 2\chi_1''\chi_3'' \\
&\quad + 2\chi_2''\chi_3'' + 2\chi_1'\chi^{\mathrm{NR}} + 2\chi_2'\chi^{\mathrm{NR}} + 2\chi_3'\chi^{\mathrm{NR}} + (\chi^{\mathrm{NR}})^2 .
\end{aligned} \tag{18}
$$

The cross terms in $|\chi^{(3)}|^2$ give rise to both destructive and constructive interferences, since χ' is an odd function. $|\chi^{(3)}|^2$ can become very complicated very quickly. The situation can be even more complicated than it may seem at first glance. Since the laser beam frequency profiles usually have considerable "tails," they can be resonant simultaneously with many Raman transitions. Although the intensity of the laser beams in these tails is quite small, the contribution to $\chi^{(3)}$ from a transition that is resonant with frequencies in the tails can be quite significant, if the population difference ΔN_{rg} is large for that transition.

When the pump and Stokes laser beams have frequency linewidths that are not small compared to the Raman transition linewidths, the CARS signal intensity given by Eq. (11) really should be written

$$
I(\omega_0) \propto \int |\chi^{(3)}|^2 I^2(\omega_1) I(\omega_2) d\omega_1\, d\omega_2 \tag{19}
$$

or

$$
I(\omega_0) \propto \int |\chi^{(3)}|^2 g(\omega_1,\omega_2;\omega_0) d\omega_1\, d\omega_2 , \tag{20}
$$

where $g(\omega_1,\omega_2;\omega_0) \equiv I^2(\omega_1) I(\omega_2)$, for $\omega_0 = 2\omega_1 - \omega_2$. In the work described here we use Eq. (20) rather than Eq. (19), for we find it easier and more reliable to determine $g(\omega_1,\omega_2;\omega_0)$ than $I(\omega_1)$ and $I(\omega_2)$ separately. The function $g(\omega_1,\omega_2;\omega_0)$ can be obtained directly from a measurement of the line shape of $I(\omega_0)$ as a function of ω_2, for an isolated (fully resolved) transition for which the Raman linewidth is much less than the laser linewidths. It is easy to find a resolved CARS transition for which the Raman linewidth is much less than the laser linewidths. At the low pressures (1 Torr or less) typical of single-collision chemical dynamics experiments the Raman linewidth is a Doppler width, and is very small due to the small transition frequency ω_{rg}. At 300 K a Raman transition at 2000 cm^{-1} for a species of mass 30 amu has a Doppler width (FWHM) of only 0.004 cm^{-1}, while our laser linewidths are typically $\sim 0.3\ \mathrm{cm}^{-1}$.

Note that Eqs. (19) and (20) involve an incoherent convolution of $I(\omega_1)I(\omega_1)I(\omega_2)$, the two-frequency-degenerate three-frequency field-intensity convolution, described by Yuratich.[12] Recently, it has been shown[13–15] that this convolution does not provide a precisely correct description of the CARS signal for the case in which a single laser beam provides both frequency-degenerate fields at ω_1, if the ω_1 laser beam is not single-axial mode and the species whose CARS spectrum is measured is present at low relative concentration ($\sim 1\%$–10%). For example, at 10% concentration of N_2 in Ar at 2000 K, the N_2 concentration determined by CARS spectroscopy using a multi-axial-mode beam at ω_1 has been found to be 14% low and the measured temperature 8% high, if the Yuratich convolution [Eq. (19)] is used in the analysis of the spectrum.[13] More accurate CARS spectral convolutions that eliminate these errors have been proposed by Teets[14] and by Kataoka, Maeda, and Hirose.[15] However, these methods increase considerably the computational time required for the solution of a problem that is already computationally intensive.

These more complicated convolutions are unnecessary for analysis of CARS spectra in chemical dynamics experiments. The errors attendant to the use of the Yuratich convolution are small compared to other measurement errors in most chemical dynamics experiments. For example, an 8% temperature error for N_2 at 2000 K corresponds to a difference of only 1 in the most probable rotational quantum number ($J = 18$ at 2000 K, $J = 19$ at 2160 K), and a change of only 1 in the FWHM of the rotational state distribution ($\Delta J_{\mathrm{FWHM}} = 30$ at 2000 K, $\Delta J_{\mathrm{FWHM}} = 31$ at 2160 K). In most chemical dynamics experiments such small differences in quantum state distributions are difficult if not impossible to discern. Furthermore, absolute concentration measurements are seldom made in chemical dynamics experiments. When they are made, they typically have errors which are much more significant than those associated with using the incoherent convolution to describe the CARS spectrum.

The unknowns to be solved for in deconvoluting an incompletely resolved CARS spectrum are the population differences ΔN_{rg} of Eq. (15). Writing Eq. (16) explicitly in terms of ΔN_{rg} we have

$$
\chi^{(3)} = \sum_{j=1}^{n} (A_j \Delta N_j + iB_j \Delta N_j) + \chi^{\mathrm{NR}} . \tag{21}
$$

Here A_j and B_j contain everything but the ΔN_j in Eqs. (13) and (14), respectively. The CARS signal then can be written explicitly in terms of the ΔN_j of Eq. (21):

$$
\begin{aligned}
I(\omega_0) \propto \int & g(\omega_1,\omega_2;\omega_0) \\
& \times \left| \sum_{j=1}^{n} (A_j \Delta N_j + iB_j \Delta N_j) + \chi^{\mathrm{NR}} \right|^2 d\omega_1\, d\omega_2 .
\end{aligned} \tag{22}
$$

The CARS spectrum is a measurement of $I(\omega_0)$ as a function of ω_2 for fixed ω_1. Measurement of $I(\omega_0)$ at any n values of the pair ω_0,ω_2 which satisfy Eq. (7) can be used to give n different equations of the form Eq. (22), which can be used to solve for the n ΔN_j. To provide the optimum sensitivity to all n ΔN_j it is best to use the values of $I(\omega_0)$ at the n pairs ω_0,ω_2 which satisfy Eq. (8) for the n Raman resonances.

The deconvolution of the CARS spectrum to get the quantum state population differences, the ΔN_{rg}, is the subject of this publication. However, we note here that the quantum state populations, which are the desired quantities, are obtained from the population differences via Eq. (15), using appropriate boundary conditions. These boundary conditions are imposed by experimental observations and/or energy and momentum conservation.

Although it does not bear directly on the computational methodology described here, we also should mention the effect that the dependence of the CARS signal on Raman transition linewidth Γ_{rg} has on the analysis. The transition linewidth is a Doppler width under the low pressure gas phase conditions of these chemical dynamics experiments.

Because of the small transition frequencies the Raman Doppler widths are quite small, less than 0.1 cm^{-1}, even for light molecules at high temperature. For example, the Doppler linewidth for H_2 at 3000 K is 0.098 cm^{-1}. Thus the Raman linewidths are smaller or much smaller than the linewidths ($\sim$0.3 cm^{-1}) of the lasers used to effect the CARS spectroscopy. However, even in such cases the magnitude of Γ_{rg} can affect the CARS signal, due to the parametric dependence of χ' and χ'' on Γ_{rg} [cf. Eqs. (13) and (14)]. For example, in a spectrum with no nonresonant background the peak CARS signal at a resonance will scale as Γ_{rg}^{-1}.[1,3–6]

For photofragments and reaction products produced under single-collision conditions Γ_{rg} is not a "normal" Doppler width, because the velocity distribution of the molecules is not Boltzmann. However, molecules in each quantum state have a specific distribution of velocities in magnitude and direction which gives a line shape that is very similar to the usual Doppler profile.[1,3–6] The conditions of the particular experiment determine the width of this line profile, and thus Γ_{rg}, for each molecular quantum state. Since the magnitude of Γ_{rg} influences the CARS signal that results from a given value of ΔN, knowledge of Γ_{rg} is necessary for solution of Eq. (22).

III. METHOD OF SOLUTION

Equation (22) relates the quantum state population differences, ΔN_k, $k = 1, 2, ..., n$ for n different pairs of quantum states, to the measured CARS signal intensity $I_k(\omega_0)$ $k = 1, 2, ..., n$ at the n values of the pair ω_0, ω_2 corresponding to the n Raman transitions. This represents a nonlinear system of n Fredholm integral equations of the first kind. This nonlinear system of equations can be solved numerically, using the damped Newton's method for nonlinear systems.[16] We write the experimentally measured intensities at the n Raman resonances as

$$\begin{aligned} I_1 &= I[\omega_0 = \omega_0(1)], \\ I_2 &= I[\omega_0 = \omega_0(2)], \\ I_n &= I[\omega_0 = \omega_0(n)], \end{aligned} \tag{23}$$

where

$$\omega_0(k) = 2\omega_1 - \omega_2(k) \tag{24}$$

and

$$\omega_1 - \omega_2(k) = \omega_{rg}(k). \tag{25}$$

For a given set of ΔN_k, a set of calculated signal intensities at the n Raman resonances is given by [cf. Eq. (22)]

$$\begin{aligned} I'[\omega_0 = \omega_0(k)] = I'_k = a \int g[\omega_1, \omega_2(k); \omega_0(k)] \\ \times \left| \sum_{j=1}^{n} (A_j \Delta N_j + iB_j \Delta N_j + \chi^{NR} \right|^2 \\ \times d\omega_1 \, d\omega_2(k). \end{aligned} \tag{26}$$

Here a is a collection of numerical constants and spectroscopic parameters.

The damped Newton's method provides a quadratically convergent iterative solution to this system of nonlinear equations. In Newton's method the mth values of the ΔN_k are given in terms of the $(m-1)$th values as

$$\begin{aligned} \Delta\mathbf{N}^{(m)} &= \Delta\mathbf{N}^{(m-1)} - \mathbf{J}^{-1}(\Delta\mathbf{N}^{(m-1)})[\mathbf{I}'(\Delta N^{(m-1)}) - \mathbf{I}] \\ &= \Delta\mathbf{N}^{(m-1)} - \Delta(\Delta\mathbf{N})^{(m-1)}, \end{aligned} \tag{27}$$

where $\Delta\mathbf{N}$ is the vector $[\Delta N_1, \Delta N_2, \Delta N_3, ..., \Delta N_n]$ and $\mathbf{I}'(\Delta\mathbf{N})$ is the vector $[I'_1, I'_2, I'_3, ..., I'_n]$. $\mathbf{J}(\Delta\mathbf{N})$ is a Jacobian whose inverse relates the errors in the $(m-1)$th calculation of the signal intensity to the correction to the $(m-1)$th values of the ΔN_k. This Jacobian is

$$\mathbf{J}(\Delta\mathbf{N}) = \begin{bmatrix} \frac{\partial(I'_1 - I_1)}{\partial\Delta N_1} & \frac{\partial(I'_1 - I_1)}{\partial\Delta N_2} & \cdots & \frac{\partial(I'_1 - I_1)}{\partial\Delta N_n} \\ \frac{\partial(I'_2 - I_2)}{\partial\Delta N_1} & \frac{\partial(I'_2 - I_2)}{\partial\Delta N_2} & \cdots & \frac{\partial(I'_2 - I_2)}{\partial\Delta N_n} \\ \vdots & \vdots & & \vdots \\ \frac{\partial(I'_n - I_n)}{\partial\Delta N_1} & \frac{\partial(I'_n - I_n)}{\partial\Delta N_2} & \cdots & \frac{\partial(I'_n - I_n)}{\partial\Delta N_n} \end{bmatrix} \tag{28}$$

Newton's method is damped by limiting the magnitude of the correction $\Delta(\Delta\mathbf{N})^{(m-1)}$, to avoid oscillation about the true solution from iteration to iteration.

We have written a Fortran 77 code that uses this damped Newton's method to solve for the ΔN_k. A simple flow diagram of the program is shown in Fig. 1. The principal input for the program is the experimental CARS spectrum $I(\omega_0)$, which is a vector of up to several thousand val-

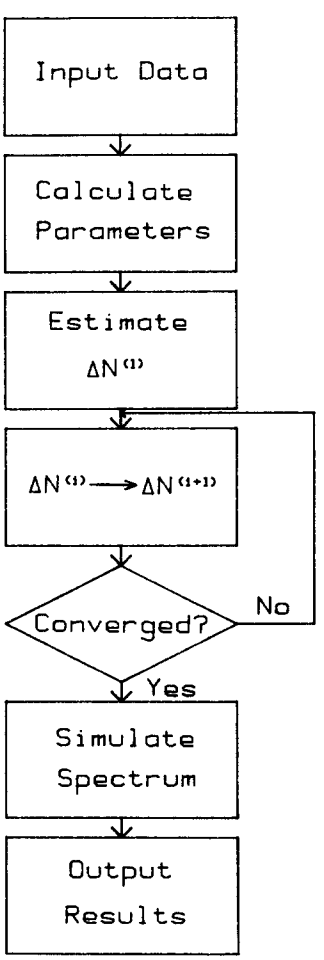

FIG. 1. Flow diagram for the computer program that analyzes incompletely resolved CARS spectra.

ues of signal intensity at a corresponding number of values of ω_0. Other input data include the nonresonant background signal $I^{NR}(\omega_0)$, also a vector of signal intensity, the laser line shape function $g(\omega_1,\omega_2;\omega_0)$, the spectroscopic constants necessary to calculate the Raman transition frequencies, and parameters like the Raman cross sections, which are necessary to relate $\Delta\mathbf{N}$ to $\mathbf{I}'(\Delta\mathbf{N})$ through the integral of Eq. (26). Typically, for vibrational Q-branch spectra we need to consider 10 to 30 Raman resonances in $\mathbf{I}'(\Delta\mathbf{N})$ and $\Delta\mathbf{N}$. However, the program provides for automatic dimensioning of all arrays, and can handle a much greater number of resonances for cases in which line spacings in the Raman spectrum are quite small.

The program calculates the values of ω_0 for the Raman resonances, based on the input spectroscopic constants. The experimental values of $I(\omega_0)$ at these resonances are determined from the $I(\omega_0)$ input vector using clamped cubic spline interpolation.[17] This is necessary, since the values of ω_0 at which $I(\omega_0)$ is experimentally measured may not include all or any of the exact values of ω_0 at which the Raman resonances occur. An initial estimate for $\Delta\mathbf{N}$ is determined by the program or can be supplied as input data.

From the initial estimate of $\Delta\mathbf{N}$, $\Delta\mathbf{N}^{(1)}$, the initial calculated spectral intensities at the Raman resonances are computed using Eq. (26). This integration is carried out numerically using composite Simpson's rule integration.[17] From the error $\mathbf{I}'(\Delta\mathbf{N}^{(1)}) - \mathbf{I}$ an improved set of population differences $\Delta\mathbf{N}^{(2)}$ is generated using Eq. (27). The Jacobian $\mathbf{J}(\Delta\mathbf{N})$ typically is of dimension 10×10 to 30×30. To avoid time-consuming inversion of $\mathbf{J}(\Delta\mathbf{N})$, we do not use $J^{-1}(\Delta N^{(1)})$ to compute $\Delta(\Delta\mathbf{N})^{(1)}$. Rather, we find $\Delta(\Delta\mathbf{N})^{(1)}$ by solving

$$\mathbf{J}(\Delta\mathbf{N}^{(1)})\Delta(\Delta\mathbf{N})^{(1)} = \mathbf{I}'(\Delta\mathbf{N}^{(1)}) - \mathbf{I}. \tag{29}$$

The improved values $\Delta\mathbf{N}^{(2)}$ are used to calculate an improved $\mathbf{I}'(\Delta\mathbf{N}^{(2)})$, and the above process repeated iteratively, until $\mathbf{I}'(\Delta\mathbf{N}) - \mathbf{I}$ converges. Convergence is determined by comparing the error

$$\left[\sum_{k=1}^{n}(I'_k - I_k)^2 \Big/ \sum_{k=1}^{n} I_k^2\right]^{1/2}$$

to a criterion of convergence provided as input.

Upon convergence the derived values ΔN_k are output along with I'_k and I_k. In addition, these ΔN_k are used to calculate, using Eq. (26), the CARS spectrum $I'(\omega_0)$ at every value of ω_0 for which the experimental signal intensity $I(\omega_0)$ was input. The calculated $[I'(\omega_0)]$ and experimental $[I(\omega_0)]$ spectra are printed out in tabular form, as well as in a line printer plot.[18]

IV. APPLICATION OF THE METHOD

We will show the utility of this program by giving the results of its use on several different CARS spectra. Relative quantum state population distributions were found from these CARS spectra. In the cases where these distributions were Boltzmann, temperatures were determined. The spectra were obtained using a conventional scanning CARS apparatus. It consists of a pulsed Nd:YAG/dye laser (Quanta-Ray DCR-2A and PDL-2) system. Part of the second harmonic output of the Nd:YAG laser is used for ω_1. The remainder of ω_1 is used to pump the tunable dye laser that generates ω_2. Typical pulse energies are 10 mJ at ω_1 and 4 mJ at ω_2, in 6 ns FWHM pulses.

The first spectrum we analyzed was that from a static, low pressure (1 Torr) sample of oxygen at ambient temperature. The observed $v = 0$ Q-branch spectrum and the spectrum calculated by the program are shown in Fig. 2. The calculated spectrum nearly exactly reproduces the observed spectrum. The laser line shape convolution function $g(\omega_1,\omega_2;\omega_0)$ used in the analysis [cf. Eq. (20)] was obtained by fitting a Gaussian-plus-Lorentzian function to an isolated, i.e., fully resolved CARS transition. The FWHM of this $g(\omega_1,\omega_2;\omega_0)$ is 0.4 cm^{-1}. Our analysis of this CARS spectrum took 40 CPU min on a VAX 11/780 using the VMS operating system. Six iterations were required to converge to a relative error, defined above, of 6×10^{-7}. A considerable amount of the execution time (25 CPU min) was used in computing the simulated spectrum, since for this Eq. (26) had to be integrated numerically for each of the 800 input values of $I(\omega_0)$.

The O_2 rotational state populations in $v = 0$ derived from the program were fit by a least-squares procedure to a Boltzmann temperature. The best fit temperature was 298 K with an uncertainty of $\pm$ 5 K. The temperature derived by our analysis is in good agreement with the actual sample temperature of 295 K. The Boltzmann plot of the O_2 rotational state populations derived from our analysis of the CARS spectrum of Fig. 2 is shown in Fig. 3. Since the O_2 sample for which the spectrum was obtained is at thermal equilibrium, the Boltzmann plot should be linear. The linear regression analysis best fit to the Boltzmann plot shows that the measured distribution is linear. The correlation coefficient of the fit was 0.997. Nothing in our CARS spectral analysis program requires that the derived O_2 rotational state populations follow a Boltzmann function. The derived populations do so only because our program accurately recovers each individual rotational state population. The $v = 0$ rotational populations $N_J \equiv N(0, J)$ used in Fig. 3 are extracted from the $\Delta N(0, J) \equiv N(0, J) - N(1, J)$ obtained by

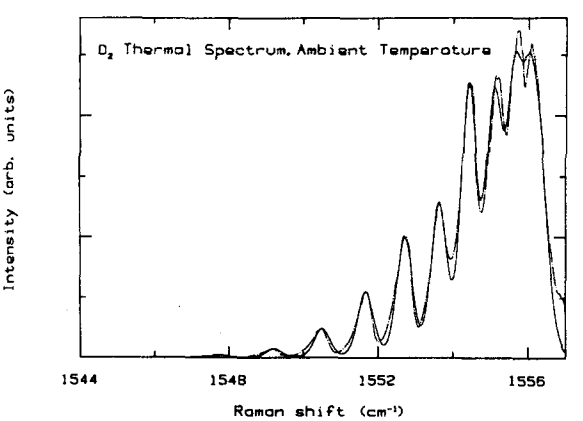

FIG. 2. Dot–dash line—observed vibrational Q-branch CARS spectrum of O_2 at 1 Torr pressure and 295 K. Solid line—calculated CARS spectrum of O_2 derived from the solution of Eq. (22) by the spectral analysis program described here, see the text for details.

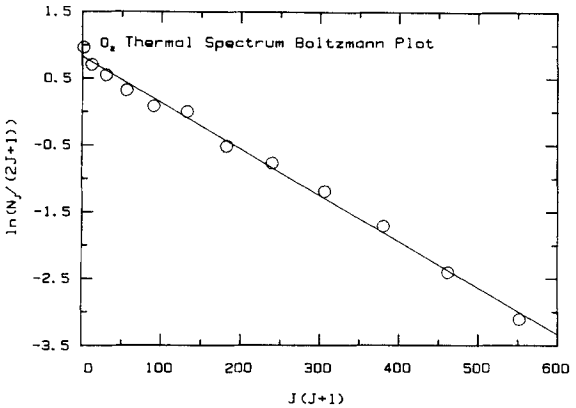

FIG. 3. Boltzmann plot of the O_2 rotational state populations derived from the CARS spectrum of Fig. 2 by the CARS spectral analysis program described here. The solid line is the linear regression analysis best fit to the rotational state populations. This fit gives a temperature of 298 K, with a correlation coefficient of 0.997. Note that for O_2 at 295 K $N(1,J) < 10^{-3}N(0,J)$ for all J, so $\Delta N(0,J) \equiv N(0,J) - N(1,J) = N(0,J)$.

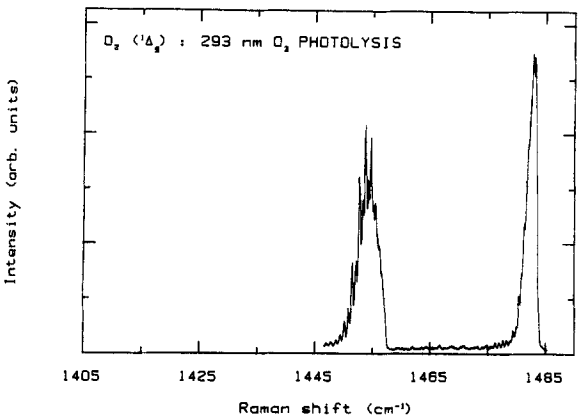

FIG. 4. Vibrational Q-branch CARS spectrum of $O_2(^1\Delta_g)$ formed in the photolysis of O_3 at 293 nm. The $v = 0$ band is at 1483 cm^{-1} and the $v = 1$ band at 1454 cm^{-1}.

the CARS spectral analysis program using the boundary condition $N(1,J) = 0$. At 295 K $N(1,J) < 10^{-3}N(0,J)$ for all J so the approximation $N(1,J) = 0$ is a good one, and $N(0,J) = \Delta N(0,J)$.

When the CARS spectrum is not as well resolved, the analysis becomes more difficult, since more cross terms in $|\chi^{(3)}|^2$ become significant. Even so, accurate analysis is still possible. To demonstrate this, we have taken CARS spectra of pure O_2 under conditions similar to those for the spectrum of Fig. 2, except at lower spectral resolution, 1.2 cm^{-1} FWHM of $g(\omega_1,\omega_2;\omega_0)$. The spectral resolution is degraded to 1.2 cm^{-1} by removing the intracavity etalon from the Nd:YAG laser. At 1.2 cm^{-1} resolution the O_2 vibrational Q branch cannot be resolved rotationally at all, and the CARS spectrum shows none of the peak structure of Fig. 2. A CARS spectrum without any structure is in principle more difficult for our analysis program to deconvolute, because at no value of ω_0 is there a single dominant term in $|\chi^{(3)}|^2$. Hence there is no $I(\omega_0)$ which is dependent primarily on only one ΔN_j. Nonetheless, our analysis program performs the deconvolution accurately. Analysis of these rotationally unresolved CARS spectra taken at ambient temperature yields Boltzmann rotational population distributions, giving temperatures within 10 K of the correct value. Significantly, the program converges to the same rotational populations regardless of what initial estimates of the populations are used.

For the pure O_2 CARS spectra discussed above, the nonresonant background is essentially zero, i.e., χ', $\chi'' \gg \chi^{NR}$. However, the program is not limited to the analysis of CARS spectra without nonresonant background. It does have an option which allows solution for the more general case in which the nonresonant background is not negligible. To demonstrate this, we obtained CARS spectra under the same experimental conditions as for the spectrum of Fig. 2. However, we added N_2 to the O_2, to generate a nonresonant background signal of about the same magnitude as the peak resonant CARS signal from O_2. Analysis of such spectra gave an O_2 rotational state distribution with a temperature within 5 K of that obtained by analysis of the spectrum of Fig. 2.

In order to demonstrate the accuracy of our CARS spectral deconvolution method it is necessary to analyze spectra for which the quantum state distribution is already known. This is the reason for analyzing the thermal equilibrium spectra shown above. However, the motivation for develop-

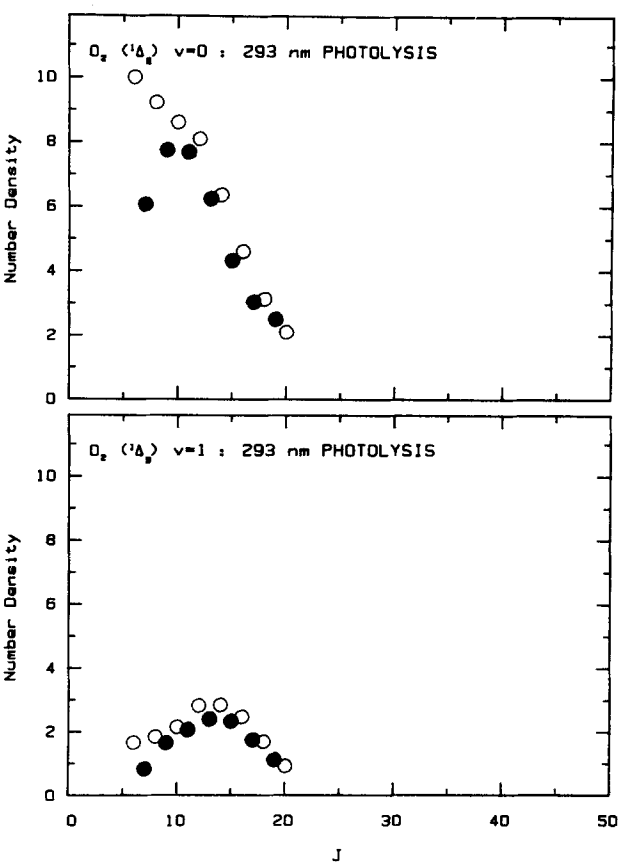

FIG. 5. Vibrational–rotational state distributions of O_2 $(^1\Delta_g)$ photofragment derived by analysis of the CARS spectrum of Fig. 4. The boundary condition $N(2,J) = 0$ for all J is used to obtain $N(1,J)$ and $N(0,J)$ from the $\Delta N(v,J) \equiv N(v,J) - N(v+1,J)$ obtained by the analysis program, see the text for details. Open circles are for even J states, filled circles for odd J states.

ing a means of analyzing incompletely resolved CARS spectra that treats individual quantum state populations as independent is to allow analysis of spectra from nonequilibrium samples. To illustrate its use for such spectra, the program was applied to a spectrum of $O_2(^1\Delta_g)$ produced by the photolysis of ozone at 293 nm. The form of the quantum state population distribution for the $O_2(^1\Delta_g)$ photofragment is not known. However, we should see a preference for even rotational states over odd rotational states by a factor of ~ 1.3, due to a dynamical bias in the photodissociation.[19] Although taken with a resolution of 0.4 cm^{-1}, neither the $v = 0$ nor the $v = 1$ Q-branch bands are very well resolved in the $O_2(^1\Delta_g)$ spectrum shown in Fig. 4, due to the close spacing of rotational lines. The rotational–vibrational state distribution obtained by our analysis of this spectrum is given in Fig. 5. This quantum state distribution clearly reveals the anticipated propensity for even J states by a factor of ~ 1.3. This quantum state distribution, $N(v, J)$ for $v = 0$ or 1, is obtained from the $\Delta N(v, J) \equiv N(v, J) - N(v + 1, J)$ using the boundary condition $N(2, J) = 0$ for all J. This boundary condition is imposed by energy conservation. Without using the CARS spectral deconvolution program described here, it would be extremely difficult to extract the $O_2(^1\Delta_g)$ quantum state population distribution from this spectrum. As Fig. 6 shows, the spectrum our program calculates using these quantum state populations is in very good agreement with the observed spectrum.

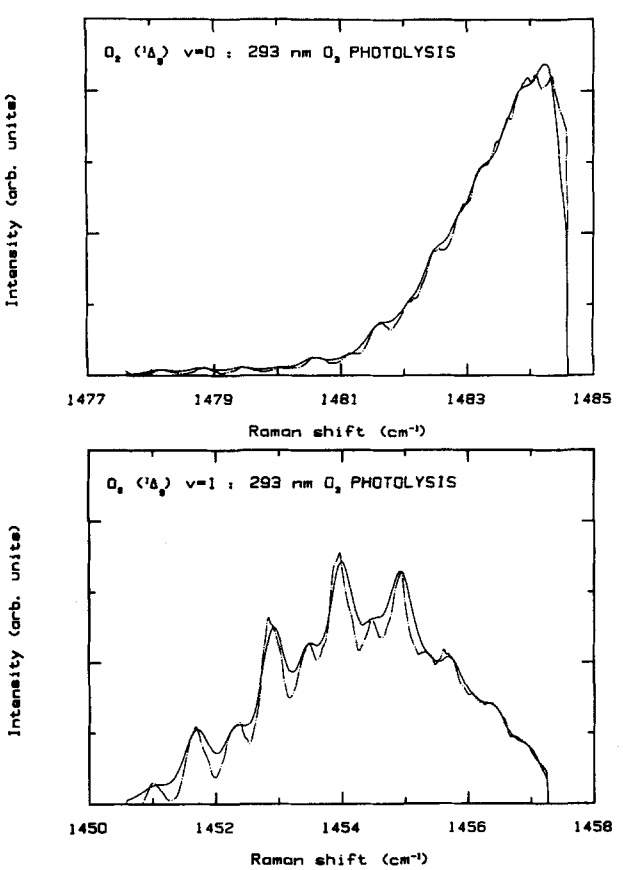

FIG. 6. Comparison of the observed $O_2(^1\Delta_g)$ photofragment CARS spectra of Fig. 4 (dot–dash line) and that calculated by the spectral analysis program described here (solid line).

V. CONCLUSION

The damped Newton's method[16] for nonlinear systems and Simpson's composite integration[17] can be used to solve the Fredholm integral equation of the first kind that describes the signal in incompletely resolved CARS spectra. This method allows determination of accurate quantum state population distributions from CARS spectra, without any assumption about the form of the population distribution. A computer code which incorporates this method of CARS spectral deconvolution has been described, and examples of its application have been presented. The accuracy of the method is demonstrated by the ability of this code to extract population distributions that are characterized by the correct temperature, for spectra taken under conditions of thermal equilibrium at known temperature. The program is most useful however, when applied to the analysis of incompletely resolved CARS spectra taken under nonequilibrium conditions, for which the form of the population distribution is unknown. This makes the code particularly useful for the analysis of CARS spectra obtained in chemical dynamics experiments, for example, CARS spectra of photofragments and reaction products.

ACKNOWLEDGMENT

This work is supported by the U. S. Department of Energy, Office of Basic Energy Sciences, through Grant No. DE-FG03-85ER13453.

[1]For a review of CARS see J. J. Valentini, in *Spectrometric Techniques*, edited by G. A. Vanasse (Academic, New York, 1985), Vol. 4, Chap. 1.
[2]J. J. Valentini, Chem. Phys. Lett. **96**, 395 (1983).
[3]D. S. Moore, D. S. Bomse, and J. J. Valentini, J. Chem. Phys. **79**, 1745 (1983).
[4]D. P. Gerrity and J. J. Valentini, J. Chem. Phys. **81**, 1298 (1984).
[5]D. P. Gerrity and J. J. Valentini, J. Chem. Phys. **82**, 1323 (1985).
[6]D. P. Gerrity and J. J. Valentini, J. Chem. Phys. **83**, 2207 (1985).
[7]R. J. Hall, Combust. Flame **35**, 47 (1979).
[8]M. P. Bogaard and B. J. Orr, in *International Review of Science. Physical Chemistry*, edited by A. D. Buckingham (Butterworths, London, 1975), Ser. 2, Vol. 2.
[9]J. A. Armstrong, N. Bloembergen, J. Ducuing, and P. S. Pershan, Phys. Rev. **127**, 1918 (1962).
[10]C. Kittel, *Introduction to Solid State Physics* (Wiley, New York, 1971).
[11]R. Pantell and H. Puthoff, *Fundamentals of Quantum Electronics* (Wiley, New York, 1969).
[12]M. A. Yuratich, Mol. Phys. **38**, 625 (1979).
[13]R. L. Farrow and L. A. Rahn, J. Opt. Soc. Am. B **2**, 903 (1985).
[14]R. E. Teets, Opt. Lett. **9**, 226 (1984).
[15]H. Kataoka, S. Maeda, and C. Hirose, Appl. Spectrosc. **36**, 565 (1982).
[16]S. D. Conte and C. deBoor, *Elementary Numerical Analysis, an Algorithmic Approach*, 3rd ed. (McGraw-Hill, New York, 1980).
[17]R. L. Burden, J. D. Faires, and A. C. Reynolds, *Numerical Analysis*, 2nd ed. (Prindle, Weber, and Schmidt, Boston, 1981).
[18]E. I. Organick and L. P. Meissner, *Fortran IV*, 2nd ed. (Addison–Wesley, Reading, Mass., 1974).
[19]D. L. Phillips, J. -C. Nieh, K. T. Tabor, D. P. Gerrity, and J. J. Valentini (to be published).